INTERNATIONAL JOURNAL FOR NUMERICAL METHODS IN FLUIDS, VOL. 10, 179–197 (1990)

A DESIGN METHOD FOR TURBOMACHINERY BLADING IN THREE-DIMENSIONAL FLOW

W. S. GHALY

Ghaly Consultants Enr., 3215 Madere Street, Brossard, Quebec, Canada J4Y 1T4

SUMMARY

A mixed spectral finite element scheme for the implementation of a design method for turbomachinery blading in three-dimensional subcritical compressible flow is presented. The method gives the detailed blade shape that would produce a prescribed tangential mean swirl schedule, given the hub and shroud profiles, the number of blades and their stacking position. After a presentation of the mathematical formulation of the design theory, the current numerical approach is described. It is then applied to the design of blading for radial inflow turbine impellers in three-dimensional flow.

KEY WORDS Inverse problem Blade design Turbomachines Finite elements Aerodynamic design Subsonic flow

INTRODUCTION

There are two approaches to solving the flow in a turbomachine. In the first one, known as the direct problem, the geometric configuration is specified and the flow and pressure fields are sought. The second approach, called the design (indirect or inverse) problem, is based on specifying part of the geometry and part of the flow or pressure field, and the solution provides the remaining part.

The theory upon which the present approach to the design problem is based has been recently published.[1–3] The flow is assumed to be steady and irrotational, the fluid is inviscid and incompressible. The blades are assumed to be infinitely thin and are set at zero incidence angle. The blades are represented by sheets of bound vorticity. The Clebsch approach is used to kinematically decompose the flow field into a potential and a rotational part. The latter is related to a function of the blade shape and the tangential average swirl schedule, which is prescribed at present and is assumed to be of the free vortex type. The blades are determined iteratively from the blade boundary condition, which requires that there should be no flow normal to the blades.

This approach was demonstrated to work in the two-dimensional limit as well. Hawthorne *et al.*[1] used it to design a two-dimensional cascade in the blade-to-blade plane, and in the meridional plane[4] with allowance for compressibility and rotationality, although no numerical examples were given in that work. Dang and McCune[5] allowed for blade thickness in the blade-to-blade plane. Dang[6] also solved the three-dimensional design problem in a rectilinear cascade allowing for rotationality. Recently, Borges[7] allowed for arbitrary hub and shroud profiles; his work was confined to incompressible flow using a multigrid finite difference technique.

In this work, the analytical theory of blade design[1–3] is extended to allow for compressibility and, to first order, for blade thickness. The numerical implementation of this design method for arbitrary hub and shroud profiles is then discussed in the subsonic flow regime. This implementation involves the use of Fourier series to take advantage of the flow periodicity in the tangential

0271–2091/90/020179–19$09.50

Received 3 November 1988
Revised 21 April 1989

direction. Since the finite element method can easily handle complex boundaries, it is used to numerically solve the relevant equations for the resulting Fourier harmonics in which the spatial dependence corresponds to that in the meridional plane. The blade surface is determined from the blade boundary condition, which yields a convective equation along the streamlines. Since the problem is non-linear, the solution is obtained iteratively. The blade thickness is represented by a mean stream surface thickness parameter. The numerical scheme is then described. The design of two radial inflow turbine impellers is used to demonstrate the application of this new technique.

2. ANALYTICAL FORMULATION

2.1. Governing equations

We consider a steady irrotational flow of an inviscid non-heat-conducting ideal gas or liquid in a radial impeller of arbitrary hub and shroud profiles, rotating at an angular speed ω. A diagrammatic sketch of a typical low-speed inflow radial turbine impeller, the co-ordinate system, the domain of interest and the notation are shown in Figure 1.

With the above assumptions and in the absence of shocks, the flow may be considered homentropic and homenergetic (the entropy Se and the rothalpy H_t^* are constant everywhere in the flow field). Thus the continuity, Crocco and energy equations and the equation of state may be written respectively as

$$\nabla \cdot \rho \mathbf{W} = 0, \tag{1}$$

$$\mathbf{W} \times \boldsymbol{\Omega} = \nabla H_t^* - T \nabla Se = 0, \tag{2}$$

$$H_t^* \equiv H_t - \omega r V_\theta = \text{constant}, \tag{3}$$

$$P = \rho R T, \tag{4}$$

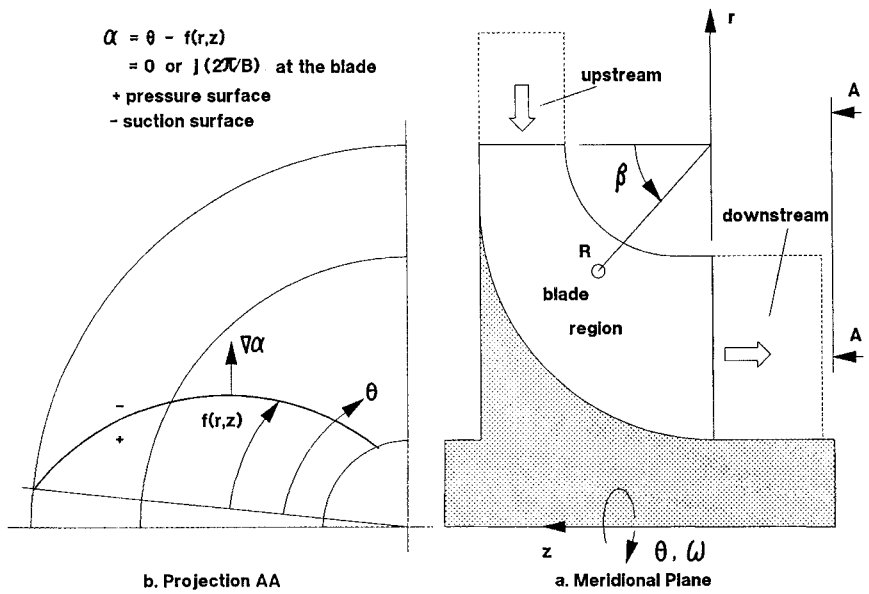

Figure 1. Schematic diagram of a radial inflow turbine impeller

and, for a homentropic flow of an ideal gas (thermally and calorically perfect), the isentropic relation holds so that

$$\left(\frac{P}{P_t^*}\right) = \left(\frac{\rho}{\rho_t^*}\right)^{\gamma} = \left(\frac{T}{T_t^*}\right)^{\gamma/(\gamma-1)}, \tag{5}$$

where P, ρ and T are the fluid pressure, density and temperature respectively, $\mathbf{V}$ is the velocity vector in the absolute frame of reference, $\mathbf{W}$ is the velocity vector relative to the impeller ($\mathbf{W}=\mathbf{V}-\omega r\mathbf{e}_\theta$), $\boldsymbol{\Omega}$ is the vorticity vector, H_t^* and H_t are the rothalpy and total enthalpy respectively ($H_t=H+0{\cdot}5V^2$), H is the static enthalpy, γ is the ratio of specific heats at constant pressure and at constant volume, $\omega r\mathbf{e}_\theta$ is the impeller velocity and (r, θ, z) denotes the right-handed cylindrical co-ordinate system.

In the limit of an imcompressible fluid flow ($\rho=$constant) the density drops out from the continuity equation and H is replaced by P/ρ in the momentum and energy equations.

2.2. The Clebsch approach

In the Clebsch formulation the velocity is kinematically decomposed into a potential and a rotational part in the following form:[8]

$$\mathbf{V} = \nabla\phi + \sigma\nabla\tau, \tag{6}$$

where $\phi(r, \theta, z)$, $\sigma(r, \theta, z)$ and $\tau(r, \theta, z)$ are the Clebsch variables. In the present problem they can be identified with the mean swirl schedule and a function of the blade shape so that the vorticity field $\boldsymbol{\Omega}$ may be written as[2,9]

$$\boldsymbol{\Omega} \equiv \nabla \times \mathbf{V} \tag{7a}$$

$$= \nabla\sigma \times \nabla\tau \tag{7b}$$

$$= \nabla r\bar{V}_\theta \times \nabla\alpha\,\delta_p(\alpha), \tag{7c}$$

where the blade surface α can, without loss of generality, be written (e.g. in the blade region) as

$$\alpha(r, \theta, z) = \theta - f(r, z) = \pm j(2\pi/B). \tag{8}$$

In equation (8), j is an integer and B is the number of blades (see Figure 1). The $\delta_p(\alpha)$ in equation (7c) is the periodic delta function[10] given as

$$\delta_p(\alpha) = \sum_{j=-\infty}^{j=+\infty} e^{ijB\alpha}, \tag{9}$$

where $i=\sqrt{(-1)}$. The overbar ($\bar{}$) defines a tangential average or mean, so that for any variable $A(r, \theta, z)$,

$$\bar{A}(r,z) = \frac{1}{2\pi/B}\int_0^{2\pi/B} A(r,\theta,z)\,d\theta. \tag{10}$$

With the assumptions prescribed here (namely the upstream flow being assumed irrotational and the mean swirl schedule being of the free vortex type), the flow upstream and downstream of the blade row is irrotational so that all the vorticity will be contained in the blades. Thus $\boldsymbol{\Omega}$ as given in equation (7c) will represent the vorticity in the entire flow field and will vanish outside the blade.

Since the flow is periodic in the circumferential direction, it is convenient to express the flow variables as a sum of a mean part ($\bar{}$) and a periodic part ($\tilde{}$). This sum corresponds to the mathematical representation of the flow variables by a Fourier series in whic h the mean part, e.g.

$\bar{\Omega}$, is the zeroth harmonic while the periodic part $\tilde{\Omega}$ constitutes the non-zeroth harmonics. Integrating Ω given by equation (7c), the velocity field may be written as[2, 9]

$$\mathbf{V} = \nabla\phi + r\bar{V}_\theta \nabla\alpha - S(\alpha)\nabla r\bar{V}_\theta, \tag{11}$$

where the mean and periodic parts of the velocity field can be written as

$$\bar{\mathbf{V}} = \nabla\bar{\phi} + r\bar{V}_\theta\nabla\alpha, \tag{12a}$$

$$\tilde{\mathbf{v}} = \nabla\tilde{\phi} - S(\alpha)\nabla r\bar{V}_\theta \tag{13a}$$

in the blade region; and since in the upstream and downstream regions the flow field is irrotational, it follows that

$$\bar{\mathbf{V}} = \nabla\bar{\phi}, \tag{12b}$$

$$\tilde{\mathbf{v}} = \nabla\tilde{\phi}. \tag{13b}$$

In equation (13a), $S(\alpha)$ is the sawtooth function[10] given as

$$S(\alpha) = \sum_{\substack{j=-\infty \\ \neq 0}}^{j=+\infty} \frac{e^{ijB\alpha}}{ijB}. \tag{14}$$

The entire flow field, with the assumptions stated above, can now be computed in terms of the Clebsch variables $\tilde{\phi}$, $\bar{\phi}$ and α ($r\bar{V}_\theta$ being prescribed in the design problem). The governing equations for the mean flow and the periodic flow are derived in the next two subsections.

2.3. *The mean flow equations*

The continuity equation may be rewritten as

$$\nabla\cdot\mathbf{W} = -\mathbf{W}\cdot\nabla\ln(\rho/\rho_t^*), \tag{15}$$

the pitch average of which gives

$$\nabla\cdot\bar{\mathbf{V}} \equiv \nabla\cdot\bar{\mathbf{W}} = -\overline{\mathbf{W}\cdot\nabla\ln(\rho/\rho_t^*)}. \tag{16}$$

The RHS is a non-linear term which couples the periodic flow field with the mean as a result of compressibility.

For computational reasons, the mean flow is formulated in terms of the Stokes streamfunction Ψ rather than the scalar potential $\bar{\phi}$ given in equation (12). These reasons have to do with the fact that the mean streamlines are eventually needed in the solution for the blade shape. In using Ψ to describe the mean flow, it is convenient to define a fictitious 'average' density $\rho_{av}(r, z)$ ($\rho_{av} \neq \bar{\rho}$) which satisfies

$$\nabla\cdot b\rho_{av}\bar{\mathbf{V}} = 0, \tag{17}$$

where b is a prescribed mean stream surface thickness parameter; it is defined as the per cent openness of the blade passage in the θ-direction. Comparing equation (17) with equation (16) we obtain a governing equation for ρ_{av} as

$$\bar{\mathbf{V}}\cdot\nabla\ln(\rho_{av}/\rho_t^*) = \overline{\mathbf{W}\cdot\nabla\ln(\rho/\rho_t^*)} - \bar{\mathbf{V}}\cdot\nabla\ln b, \tag{18}$$

which yields the 'average' density ρ_{av} (when solved with an appropriate initial condition).

Equation (17) can now be satisfied by introducing the Stokes streamfunction $\Psi(r, z)$:

$$b\rho_{av}\bar{\mathbf{V}}_r = -\frac{\rho_t^*}{r}\frac{\partial\Psi}{\partial z}, \qquad b\rho_{av}\bar{\mathbf{V}}_z = \frac{\rho_t^*}{r}\frac{\partial\Psi}{\partial r}. \tag{19}$$

The governing equation for Ψ is obtained by equating the definition of $\bar{\Omega}_\theta$ from equation (7a) to that from equation (7c) using equation (19); this gives

$$(L-N)\Psi = -(\rho_{av}/\rho_t^*)\bar{\Omega}_\theta, \tag{20}$$

where

$$L = \frac{\partial}{\partial r}\left(\frac{1}{r}\frac{\partial}{\partial r}\right) + \frac{\partial}{\partial z}\left(\frac{1}{r}\frac{\partial}{\partial z}\right),$$

$$N = \frac{1}{r}\left(\frac{\partial \ln(b\rho_{av}/\rho_t^*)}{\partial r}\frac{\partial}{\partial r} + \frac{\partial \ln(b\rho_{av}/\rho_t^*)}{\partial z}\frac{\partial}{\partial z}\right),$$

$$\bar{\Omega}_\theta = \frac{\partial r\bar{V}_\theta}{\partial r}\frac{\partial f}{\partial z} - \frac{\partial r\bar{V}_\theta}{\partial z}\frac{\partial f}{\partial r}.$$

Equation (20) is elliptic when the flow is subsonic, and hyperbolic when the flow becomes supersonic. Note that the RHS vanishes outside the blade region since the flow is irrotational there.

The boundary conditions for equation (20) when the flow is subsonic are as follows.

1. Along the inflow and outflow sections, $\partial\Psi/\partial n = 0$.
2. Along the hub and the shroud, Ψ is constant (no flow normal to the wall).

A useful flow model, the bladed actuator duct,[2] is obtained when the number of blades B becomes infinite while $r\bar{V}_\theta$ is kept fixed. In the bladed actuator duct ($B \to \infty$) the periodic part of the flow vanishes; hence $\tilde{\mathbf{v}} = 0$, $\rho_{av} = \bar{\rho}$ and equation (18) is identically satisfied. In that limit a blade shape can still be determined as will be described in Section 2.5.

2.4. The periodic flow equation

The continuity equation for the periodic part of the flow is obtained by subtracting the pitch-averaged continuity equation (16) from the continuity equation (15) to yield

$$\nabla\cdot\tilde{\mathbf{v}} = -\mathbf{W}\cdot\nabla\ln(\rho/\rho_t^*) + \overline{\mathbf{W}\cdot\nabla\ln(\rho/\rho_t^*)}. \tag{21}$$

Substituting for $\tilde{\mathbf{v}}$ in terms of its Clebsch variables from equation (13) we obtain

$$\nabla^2\tilde{\phi} = \nabla\cdot\{S(\alpha)\nabla r\bar{V}_\theta\} - \mathbf{W}\cdot\nabla\ln(\rho/\rho_t^*) + \overline{\mathbf{W}\cdot\nabla\ln(\rho/\rho_t^*)}, \tag{22a}$$

where ∇^2 is the Laplacian. The first term on the RHS vanishes outside the blade region since the flow is assumed to be irrotational there, while the other two terms vanish in the incompressible flow limit.

The boundary conditions for equation (22a) when the flow is subsonic are as follows.

1. Along the inflow and outflow sections, $\tilde{\mathbf{v}}(=\nabla\tilde{\phi})$ is assumed to be negligibly small so that $\partial\tilde{\phi}/\partial n$ is approximately zero there.
2. Along the hub and shroud, there should be no flow normal to the wall so that

$$\frac{\partial\tilde{\phi}}{\partial n} = \begin{cases} S(\alpha)\,\partial r\bar{V}_\theta/\partial n & \text{in the blade region,} \quad (22b) \\ 0 & \text{elsewhere.} \quad (22c) \end{cases}$$

Equation (22) can be readily solved for $\tilde{\phi}(r,\theta,z)$ if the RHS is given. As mentioned earlier, because of inherent periodicity in the θ-direction, Fourier series can be used to represent the θ-dependence of any of the flow variables. Accordingly, $\tilde{\phi}$ may be approximated with a truncated

Fourier series of the form

$$\tilde{\phi}(r,\theta,z) = \sum_{\substack{j=-N \\ \neq 0}}^{j=N-1} \tilde{\Phi}_j(r,z)\, e^{ijB\theta}. \tag{23}$$

Since $\tilde{\phi}$ is real, $\tilde{\Phi}_j = \tilde{\Phi}^*_{-j}$, where * denotes the complex conjugate, so that only $\tilde{\Phi}_j$ for either positive or negative j need be computed. By substituting for $\tilde{\phi}$ from equation (23) into equation (22) and making use of the orthogonality property of the Fourier series, the following set of equations for the Fourier coefficients is obtained:

$$r\nabla^2_{2D}\tilde{\Phi}_j(r,z) = r\nabla\cdot[(1/ijB)e^{-ijBf(r,z)}\nabla r\bar{V}_\theta] - r[\mathbf{W}\cdot\nabla\ln(\rho/\rho_t^*) - \overline{\mathbf{W}\cdot\nabla\ln(\rho/\rho_t^*)}]_{FT}, \tag{24a}$$

where

$$r\nabla^2_{2D} = \frac{\partial}{\partial r}\left(r\frac{\partial}{\partial r}\right) + \frac{\partial}{\partial z}\left(r\frac{\partial}{\partial z}\right) - \frac{j^2B^2}{r}$$

and the subscript FT denotes the Fourier coefficients; however, these coefficients are evaluated using the predetermined value of that term at the chosen Fourier collocation points. This equation needs to be solved only for $j=-N$ to $j=-1$. Note that the RHS of equation (24a) vanishes when $j=0$, so that $\tilde{\Phi}_0 \equiv 0$ (with the corresponding boundary conditions) as it should, since $\tilde{\mathbf{v}} \equiv 0$ by definition.

The boundary conditions associated with equation (24a) follow from equations (22b, c). Taking into account that $\partial r\bar{V}_\theta/\partial n = 0$ along the hub and shroud,[9] these boundary conditions may be written as $\partial\tilde{\Phi}_j/\partial n = 0$ on the entire boundary. However, $\tilde{\Phi}_j = 0$ at one point is used to set the value of the arbitrary constant to zero. Hence the boundary conditions used in solving for $\tilde{\Phi}_j$ take the form of

$$\tilde{\Phi}_j = 0 \quad \text{at an inflow-shroud point,} \tag{24b}$$

$$\partial\tilde{\Phi}_j/\partial n = 0 \quad \text{elsewhere.} \tag{24c}$$

Since the source term in equation (24a) has a periodic delta function behaviour, $\tilde{\Phi}_j$ is expected to be $O(1/j^2)$; hence the truncation error in the representation of $\tilde{\phi}$, given in equation (23), would be $O(1/N^2)$. Moreover, $\nabla\tilde{\Phi}_j$ will be $O(1/j)$; therefore Gibbs' phenomenon will be encountered in evaluating $\nabla\tilde{\phi}$ and hence in calculating the velocity field. However, this fact has no serious impact on the calculation of the blade shape $f(r,z)$ since that calculation involves only the mean of the velocities on both sides of the blades which does not suffer from that phenomenon.

In summary, the flow periodicity in the θ-direction has been used to transform a three-dimensional elliptic problem, equations (22), into a set of two-dimensional ones, equations (24). Now both mean and periodic flow fields are obtained by solving numerically a set of two-dimensional elliptic equations. This is accomplished by appealing to the finite element method (FEM) for the reasons listed in Section 3.1.

2.5. The blade boundary condition

The remaining boundary condition is the blade boundary condition, which states that the velocity normal to the blade surfaces vanishes. Since $\nabla\alpha$ is normal to the blade surfaces, the blade boundary condition on the pressure and suction sides of the blades may be written as

$$\mathbf{W}^+\cdot\nabla\alpha = 0, \qquad \mathbf{W}^-\cdot\nabla\alpha = 0.$$

Adding and subtracting the above equations we obtain

$$\mathbf{W}_{bl} \cdot \nabla \alpha = 0, \tag{25a}$$

$$\Delta \mathbf{W} \cdot \nabla \alpha = 0, \tag{26}$$

where the velocity 'at' the blades is defined as $\mathbf{W}_{bl} \equiv \frac{1}{2}(\mathbf{W}^+ + \mathbf{W}^-)$ and the velocity jump across the blades is given as $\Delta \mathbf{W} = \mathbf{W}^+ - \mathbf{W}^-$. Equation (26) is identically satisfied since $\Delta \mathbf{W}$ is a measure of the bound vorticity which lies in the blade surface.

It remains to satisfy equation (25a), called the blade boundary condition.[2] This equation is solved for the blade shape $f(r, z)$; it may also be written in the form

$$\bar{\mathbf{V}} \cdot \nabla f = \bar{\mathbf{W}}_\theta / r + \tilde{\mathbf{v}}_{bl} \cdot \nabla \alpha, \tag{25b}$$

and when the number of blades $B \to \infty$, it reduces to

$$\bar{\mathbf{V}} \cdot \nabla f = \bar{\mathbf{W}}_\theta / r. \tag{25c}$$

An analogous initial condition for $f(r, z)$ in the r–z plane is needed to fix the value of the arbitrary constant in the solution of any of equations (25a–c); e.g.

$$f_{st} = f(r_{st}, z_{st}) \tag{25d}$$

may be given along a line going from hub to shroud (not coinciding with any of the streamlines). This initial condition is called the blade stacking position.[2]

We proceed to describe the Kutta condition and some kinematic constraints implied by the above formulation in the following two subsections.

2.6. *Kinematic constraint*

The fact that the flow is assumed to be irrotational and inviscid implies that[16] $\partial r\bar{V}_\theta / \partial n = 0$ along the hub and shroud (n being the unit vector normal to the hub and the shroud surface). This implication follows from relating $r\bar{V}_\theta$ to the circulation around the blade and satisfying the wall boundary condition. It results in an additional constraint on the blade shape at its intersection with the hub and shroud, namely[9] $\partial f / \partial n = 0$. This generalizes the result previously obtained by Tan *et al.*[2] to bounding walls of arbitrary geometry.

2.7. *The Kutta condition*

The Kutta condition ensures smooth flow at a sharp trailing edge. This translates to the fact that, in subsonic flow, the pressure must be continuous at the trailing edge. Accordingly, the swirl schedule should be such as to satisfy this condition. The homentropic assumption implies that all the thermodynamic properties will be continuous if either P or ρ or T is. Hence, by requiring that the enthalpy jump across the blade trailing edge vanishes, the temperature and hence the pressure will also be continuous.

Since the rothalpy is uniform, it follows that

$$H^+ - H^- = 0{\cdot}5(\mathbf{W}^-)^2 - 0{\cdot}5(\mathbf{W}^+)^2 = -\mathbf{W}_{bl} \cdot \Delta \mathbf{W}. \tag{27a}$$

Using the definition of $\mathbf{W}_{bl}$, substituting for $\Delta \mathbf{W}$ in terms of the bound vorticity and using the blade boundary condition (equation (25a)) we obtain

$$H^+ - H^- = \frac{2\pi}{B} \mathbf{W}_{bl} \cdot \nabla r\bar{V}_\theta, \tag{27b}$$

so that the Kutta condition can be directly satisfied by setting the RHS of the above equation to zero, i.e.

$$\mathbf{W}_{\mathrm{bl}} \cdot \nabla r \bar{V}_\theta = 0. \tag{28}$$

It is noteworthy that since the incidence angle at the blades' leading edge (LE) is assumed to be zero, the pressure there should be continuous in a way similar to that at the TE. Therefore the condition of zero incidence at the blades' LE implies that $r\bar{V}_\theta$ should satisfy equation (28) at the LE as well.

3. NUMERICAL TECHNIQUE

The numerical scheme adopted in solving the governing equations, namely equation (20), (24), (25b) and (18), and the computational procedure are presented in this section. The main features of (and notes on) the numerical scheme are also described.

3.1. The elliptic solver

Equation (20) for the mean streamfunction Ψ and equation (24) for the Fourier harmonics $\tilde{\Phi}_j$ of the periodic potential function are two-dimensional elliptic equations (when the flow is subsonic). Since the solution procedure is iterative, the non-linear part of the differential operator in equation (20), namely N, is taken to the RHS, which can now be assumed as given from the previous iteration or the initial guess so that, at each iteration level, the equations may be treated as linear equations.

In the present work, FEM consists of the following. A Galerkin weighted residual technique is adopted and the conventional finite element technique is applied to the resulting integral. The isoparametric formulation is adopted and a nine-node element with a biquadratic basis function is used.

At this point, a few notes on FEM are due.

1. It is well suited for domains having highly irregular boundaries. The Dirichlet boundary condition nodes need not be solved for, and the homogeneous Neumann boundary condition ($\partial/\partial n = 0$) is a natural boundary condition for FEM.
2. For the basis function used in this problem, the method is third-order accurate[11] when the elements are not distorted, i.e.

$$\Psi_{\mathrm{exact}} - \Psi_{\mathrm{numerical}} = O(l^3),$$

where l is the element characteristic dimension (e.g. its diagonal). The accuracy deteriorates[12] by 0·3–0·7 of an order depending on the amount of mesh distortion incurred.
3. For the direct solver, since the system matrix is sparse, it is efficiently stored using the skyline method.[13] It is also a well conditioned matrix so that round-off errors associated with solving it are minimal. It is solved directly by an LDU decomposition[13] done once (since the differential operators are linear) and back substitution done at each iteration level. Since the differential operators (L in equation (20) and $r\nabla^2_{2\mathrm{D}}$ in equation (24)) are self-adjoint, the resulting system matrix is symmetric, hence only half of it is stored, e.g. L, and $U = L^{\mathrm{T}}$, where L^{T} is the transpose of L.
4. For the iterative solver, since the system matrix is symmetric, sparse and well conditioned, it can be solved efficiently by the preconditioned conjugate gradient method.[14] The starting value for the unknown function is its value from the previous iteration (or zero on the first iteration).
5. Both direct and iterative solvers do not require an elaborate initial guess for the unknown function; they simply require the boundary condition.

3.2. The convection equations solver

Equation (25b) for the blade shape $f(r,z)$ and equation (18) for the average density $\rho_{av}(r,z)$ are convective equations along one set of characteristic directions, namely the streamlines as defined in equation (19). In these equations the RHS may be considered given from the initial guess or the previous iteration. The operator

$$\bar{\mathbf{V}}\cdot\nabla \equiv \bar{V}_m\,\partial/\partial m,$$

where $\bar{V}_m$ $(=(\bar{V}_r^2+\bar{V}_z^2)^{1/2})$ is the mean meridional velocity and m is the distance along the streamlines of the mean flow. Hence the convective equations (equation (25b) and (18)) for f and ρ_{av} may be written in the form

$$\bar{V}_m\frac{\partial f}{\partial m} = \bar{W}_\theta/r + \tilde{\mathbf{v}}_{bl}\cdot\nabla\alpha, \tag{29}$$

$$\bar{V}_m\frac{\partial \ln(\rho_{av}/\rho_t^*)}{\partial m} = \overline{\mathbf{W}\cdot\nabla\ln(\rho/\rho_t^*)} - \bar{V}_m\frac{\partial \ln b}{\partial m}. \tag{30}$$

The blade stacking position is implemented by prescribing f along a line going from hub to shroud. For the average density (equation (30)), the initial condition is given by $\rho_{av}=\bar{\rho}$ along the inflow section.

These equations are solved by locating the streamlines m, integrating f and ρ_{av} (equations (29) and (30)) along those streamlines and interpolating f and ρ_{av} back to the finite element mesh.

The streamlines are located as follows. Along each quasi-orthogonal line in the r–z plane (lines going from hub to shroud and normal or almost normal to them) a cubic spline[15] is fitted into the nodal values of the streamfunction Ψ so that it may be evaluated at any point along the quasi-orthogonal. The method of bisections[15] uses the cubic spline fit for Ψ to locate the different streamlines ($\Psi=$constant) crossing that quasi-orthogonal. Equations (29) and (30) are then integrated along the streamlines using the trapezoidal rule to yield f and ρ_{av}, which are interpolated back to the finite element mesh using the cubic splines once more. The success of this method in locating the streamlines relies on the fact that Ψ varies monotonously from hub to shroud, i.e. it assumes implicitly that the meridional velocity $\bar{V}_m$ does not vanish (implying a possible extremum of Ψ).

The cubic splines are fourth-order accurate (except near the splines' endpoints where they are slightly less accurate) so as to maintain the same or higher accuracy compared with that of the streamfunction Ψ (2·5–3rd-order accurate).

3.3. The computation scheme

Since the system of equations to be solved is non-linear, the solution is iterative. The iteration scheme implemented in the computer program consists of the following steps.

1. Enter the input data: the hub and the shroud profiles, the prescribed mean swirl schedule, the number of blades and their stacking position, the impeller speed and the upstream flow conditions (which are uniform).
2. Solve the mean flow equation (equation (20)) for $\Psi(r,z)$.
3. Solve the periodic flow equation (equation (24)) for $\tilde{\Phi}_j(r,z)$, the Fourier coefficients of the periodic scalar potential $\tilde{\phi}(r,\theta,z)$.
4. Solve the blade boundary condition (equation (29)) iteratively for the blade shape $f(r,z)$.

   4.1. Evaluate $\tilde{\mathbf{v}}_{bl}\cdot\nabla\alpha$ for the current α.

4.2. Solve the blade boundary condition for $f(r,z)$ and update α.
4.3. If not converged, go to step 4.1.

5. If the flow is compressible, solve for the average density (equation (30)) and use the energy and homentropic relations to calculate the density.
6. If convergence is attained, stop; otherwise go to step 2.

FEM procedures are used to evaluate all derivatives. Since ρ/ρ_t^* has a jump across the blades, its gradient will behave like a periodic delta function there. Therefore $\nabla\ln(\rho/\rho_t^*)$ is evaluated by taking a DFT of $\ln(\rho/\rho_t^*)$, evaluating the gradients in the Fourier space and then taking an IDFT back to the physical space. A fast Fourier transform[16] has been used to evaluate the DFT and the IDFT of $\mathbf{W}$ and $\ln(\rho/\rho_t^*)$ as mentioned above. Also, Lanczos smoothing[17] has been used in calculating $\mathbf{W}$ and $\ln(\rho/\rho_t^*)$ to alleviate the Gibbs phenomenon near the blade.

At this point, a note on the maximum number of harmonics (N) to be used in a certain calculation is due. The error in determining $\tilde{\phi}$ is due to truncating the series representation of $\tilde{\phi}$ and to the numerical error incurred in computing each of the harmonics $\tilde{\Phi}_j$, so that

$$\varepsilon_N \equiv \varepsilon_{\text{FEM}} + \varepsilon_{\text{truncation}} = \sum_{\substack{j=-N \\ \neq 0}}^{j=N-1} \varepsilon_j e^{ijB\theta} + \sum_{|j|>N} \tilde{\Phi}_j(r,z) e^{ijB\theta}, \tag{31}$$

where ε_j is the error incurred in computing $\tilde{\Phi}_j$. It is possible that, on a coarse mesh, ε_{FEM} will become larger than $\varepsilon_{\text{truncation}}$ even for relatively small values of N, so that the overall error ε_N would be dominated by the FEM discretization error. The number of blades (B) is an important factor in determining the size of ε_j. As B increases, the source term in equation (24) becomes more oscillatory (implying that $\tilde{\Phi}_j$ will also be a highly oscillatory function) so that the numerical accuracy deteriorates significantly. The case becomes even worse for the higher harmonics since the harmonics' absolute value ($O(1/j)$) becomes comparable with the error incurred in calculating them.

A numerical test has shown that when too many harmonics in the θ-direction are evaluated on a coarse mesh in the (r,z) plane, spurious wiggles show up in the θ-variation of $\nabla\tilde{\phi}$. In short, the number of harmonics in the θ-direction, namely N, should be such that with the given mesh size (characterized by l) in the (r,z) plane, the RHS source term in equation (24) can be integrated with acceptable accuracy.

3.4. Convergence and consistency

Convergence in this context refers to the numerical evolution of the solution from an initial guess to the final answer. It is measured by the maximum change in pointwise values of the variables, called the residual, from one global iteration to the next. The blade boundary condition given in equation (29) may be rewritten as

$$f^{i+1} \equiv I^i = \int_{m^i} [\bar{W}_\theta/r - (\mathbf{v}_{\text{bl}} \cdot \nabla\alpha)^i]/\bar{V}_{\text{m}}^i \, \mathrm{d}m^i, \tag{32}$$

where the superscripts i and $i+1$ refer to successive global iteration levels. Equation (32) can be rewritten as

$$\partial f/\partial\tau + f^i = I^i, \tag{33}$$

where $\partial f/\partial\tau \equiv (f^{i+1} - f^i)/\lambda$ is a pseudo-time derivative of f. Hence

$$f^{i+1} = \lambda I^i + (1-\lambda) f^i, \tag{34}$$

where λ is a pseudo-time step. It corresponds to one global iteration loop where the solution advances by one step from the initial guess towards the final answer; note that when $\lambda = 1$, equations (34) and (32) become identical. Equation (33) is analogous to the Euler forward integration scheme (explicit, one-step); correspondingly, λ is analogous to a time step, the upper bound of which is set by the stability requirement of the function being integrated.[18] For illustration, the convergence history for different values of λ is shown in Figure 2.

It was found that the explicit imposition of the kinematic condition at the bounding walls, namely $\partial f/\partial n = 0$ along the hub and shroud, was necessary to obtain a converged solution; this behaviour was also observed by Tan *et al.*[2]

In the course of this work it was found that a converged solution is obtainable whenever the mean meridional velocity $\bar{V}_m$ does not vanish and/or when the flow is not in the transonic regime. When $\bar{V}_m$ vanishes, equation (29) for the blade shape indicates that $\partial f/\partial m \to \infty$, which is not accounted for in the present work. On the other hand, in the transonic and supersonic flow regimes, the numerical scheme used for implementing the inverse design method must appropriately account for the change in the character of the governing equations from elliptic to hyperbolic.

The program is checked for consistency. This check is given by the kinematic identity (equation (21), Reference 2) relating the velocity jump across the blades $\Delta \mathbf{W}$ to the bound vorticity $\boldsymbol{\Omega}$. Both the RHS and LHS of this identity are evaluated independently and compared. This test is a severe one since the Gibbs phenomenon will occur in evaluating the velocity jump $\Delta \mathbf{W}$. It was found that, on average, the discrepancy between the two sides decreases as the total number of elements is increased, which agrees with the above analysis.

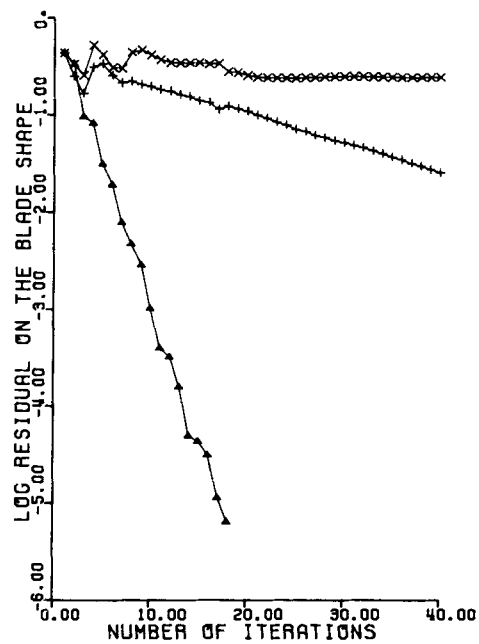

Figure 2. Convergence history for different values of pseudo-time step λ: Δ, $\lambda = 0{\cdot}5$; +, $\lambda = 1$; ×, $\lambda = 1{\cdot}25$

4. NUMERICAL EXAMPLES

To demonstrate the numerical technique presented earlier, it is applied to the design of two inflow radial turbine impellers. In these designs the kinematic variables are normalized using the radius and radial velocity at the blades' LE, and the rotary stagnation state (which is reached when the flow is isentropically decelerated to a stagnation state in the impeller frame) is used as a reference state for the thermodynamic variables.

The computational domain is discretized into 240 elements in the r–z plane having $l_{max}=0{\cdot}08$ and 1053 nodes, as shown in Figure 3, and eight harmonics in the Fourier series representation ($N=8$ in equation (23)).

In both examples the impeller rotational speed $\omega=2{\cdot}7475$ and the mean swirl schedule takes the following form:

$$r\bar{V}_\theta(r,z) = c_1(R)(a(R)\sin 2\beta + 2\cos 2\beta)\,e^{-a(R)\beta} + c_2(R), \tag{35}$$
$$\partial r\bar{V}_\theta/\partial s = -c_3(R)\,e^{-a(R)\beta}\sin 2\beta,$$

where $c_3(R)=c_1(R)(a^2(R)+4)/R$, $s=R\beta$ and R and β are shown in Figure 1. The exponent $a(R)$ varies linearly from hub to shroud, and the constants c_1 and c_2 are calculated from the values of $r\bar{V}_\theta$ set to 2·7475 and 0 at the blades' leading and trailing edges respectively. Note that the mean swirl schedule satisfies the constraints at the blades' leading and trailing edges mentioned in Section 2.7; moreover, the kinematic constraint mentioned in Section 2.6, namely $\partial r\bar{V}_\theta/\partial n=0$, is imposed by adjusting the value of $r\bar{V}_\theta$ along the hub and shroud such that this constraint is satisfied.

The first example is that of a double-circular-arc impeller (where both hub and shroud form circular arcs in the meridional plane) having 15 blades stacked at midchord. The exponent $a(R)$ in equation (35) varies linearly between 2·5 along the hub and 0·5 along the shroud, and the relative

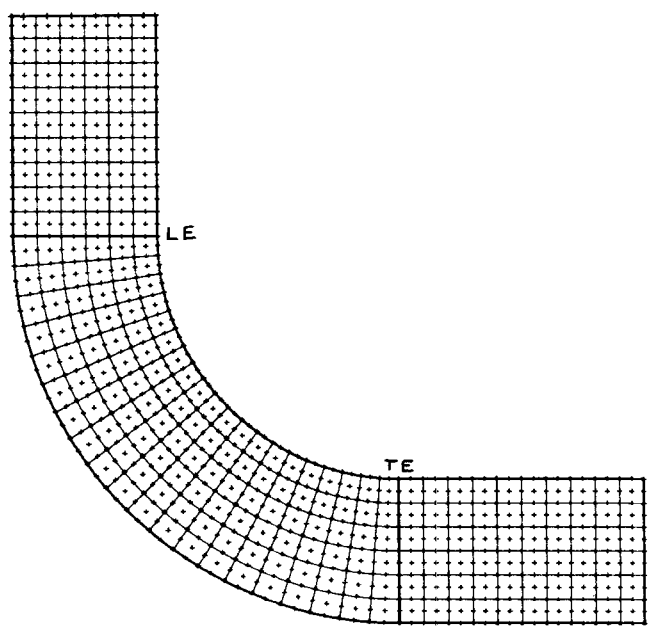

Figure 3. The finite element mesh; the nodes are marked with a + symbol

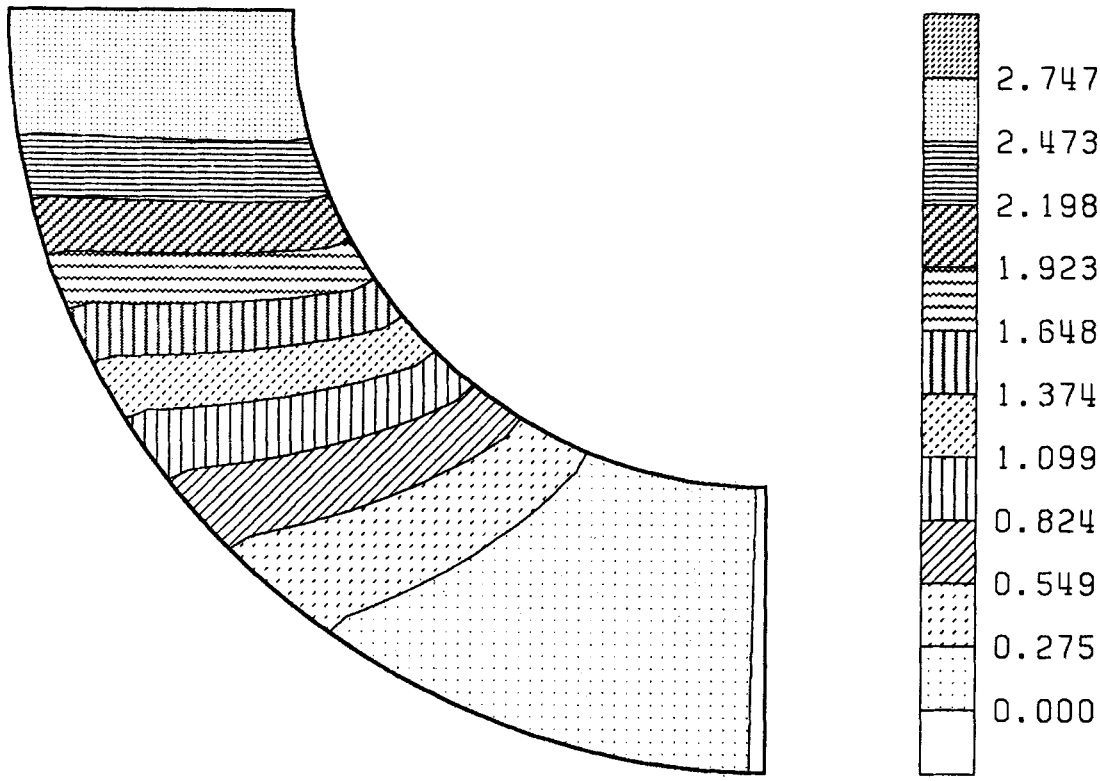

Figure 4. The mean swirl distribution $r\bar{V}_\theta$

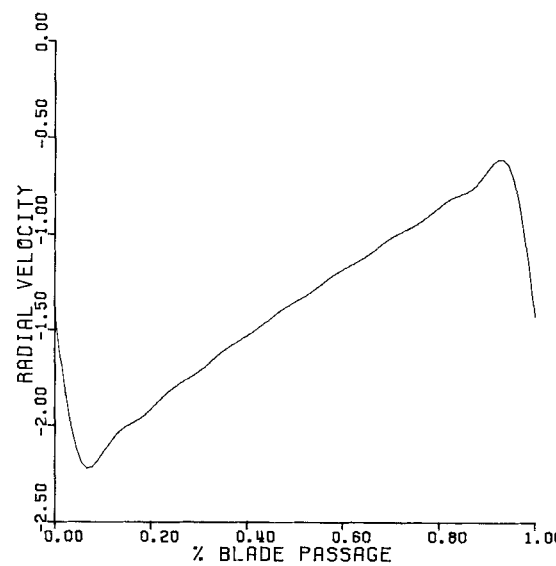

Figure 5. The relative radial velocity at midchord and midspan

Table I. The impeller geometry (r, f, z) corresponding to the first design

r	f	z	r	f	z	r	f	z
1·0000	−0·1825	0·8000	0·8439	−0·0968	0·7846	0·6939	−0·0005	0·7391
1·0000	−0·1840	0·7750	0·8488	−0·1006	0·7601	0·7034	−0·0071	0·7160
1·0000	−0·1884	0·7500	0·8537	−0·1121	0·7356	0·7130	−0·0267	0·6929
1·0000	−0·1943	0·7250	0·8586	−0·1247	0·7111	0·7226	−0·0470	0·6698
1·0000	−0·1958	0·7000	0·8634	−0·1341	0·6865	0·7321	−0·0610	0·6467
1·0000	−0·1966	0·6750	0·8683	−0·1384	0·6620	0·7417	−0·0657	0·6236
1·0000	−0·1948	0·6500	0·8732	−0·1408	0·6375	0·7513	−0·0690	0·6005
1·0000	−0·1928	0·6250	0·8781	−0·1417	0·6130	0·7608	−0·0712	0·5774
1·0000	−0·1903	0·6000	0·8829	−0·1421	0·5885	0·7704	−0·0734	0·5543
1·0000	−0·1883	0·5750	0·8878	−0·1433	0·5640	0·7800	−0·0767	0·5312
1·0000	−0·1892	0·5500	0·8927	−0·1473	0·5394	0·7895	−0·0842	0·5081
1·0000	−0·1876	0·5250	0·8976	−0·1505	0·5149	0·7991	−0·0915	0·4850
1·0000	−0·1870	0·5000	0·9025	−0·1515	0·4904	0·8087	−0·0940	0·4619
0·5555	0·0367	0·6652	0·4343	0·0000	0·5657	0·3348	−0·0721	0·4445
0·5694	0·0304	0·6444	0·4520	0·0000	0·5480	0·3556	−0·0678	0·4306
0·5833	0·0115	0·6236	0·4697	0·0000	0·5303	0·3764	−0·0550	0·4167
0.5972	−0·0057	0·6028	0·4873	0·0000	0·5127	0·3972	−0·0417	0·4028
0·6111	−0·0108	0·5820	0·5050	0·0000	0·4950	0·4180	−0·0383	0·3889
0·6250	−0·0131	0·5612	0·5227	0·0000	0·4773	0·4388	−0·0349	0·3750
0·6389	−0·0150	0·5405	0·5404	0·0000	0·4596	0·4595	−0·0315	0·3611
0·6528	−0·0168	0·5197	0·5581	0·0000	0·4419	0·4803	−0·0279	0·3472
0·6667	−0·0187	0·4989	0·5757	0·0000	0·4243	0·5011	−0·0241	0·3333
0·6805	−0·0211	0·4781	0·5934	0·0000	0·4066	0·5219	−0·0199	0·3195
0·6944	−0·0277	0·4573	0·6111	0·0000	0·3889	0·5427	−0·0106	0·3056
0·7083	−0·0353	0·4365	0·6288	0·0000	0·3712	0·5635	−0·0000	0·2917
0·7222	−0·0378	0·4157	0·6464	0·0000	0·3536	0·5843	0·0035	0·2778
0·2609	−0·1719	0·3061	0·2154	−0·2976	0·1561	0·2000	−0·4309	0·0000
0·2840	−0·1661	0·2966	0·2399	−0·2901	0·1512	0·2250	−0·4206	0·0000
0·3071	−0·1488	0·2870	0·2644	−0·2678	0·1463	0·2500	−0·3896	0·0000
0·3302	−0·1273	0·2774	0·2889	−0·2394	0·1414	0·2750	−0·3544	0·0000
0·3533	−0·1169	0·2679	0·3135	−0·2215	0·1366	0·3000	−0·3308	0·0000
0·3764	−0·1092	0·2583	0·3380	−0·2074	0·1317	0·3250	−0·3099	0·0000
0·3995	−0·1011	0·2487	0·3625	−0·1933	0·1268	0·3500	−0·2899	0·0000
0·4226	−0·0919	0·2392	0·3870	−0·1775	0·1219	0·3750	−0·2681	0·0000
0·4457	−0·0831	0·2296	0·4115	−0·1631	0·1171	0·4000	−0·2481	0·0000
0·4688	−0·0726	0·2200	0·4360	−0·1453	0·1122	0·4250	−0·2241	0·0000
0·4919	−0·0552	0·2105	0·4606	−0·1215	0·1073	0·4500	−0·1952	0·0000
0·5150	−0·0363	0·2009	0·4851	−0·0960	0·1024	0·4750	−0·1648	0·0000
0·5381	−0·0299	0·1913	0·5096	−0·0875	0·0975	0·5000	−0·1547	0·0000

Mach number at the blades' LE is set to 0·15 (based on a mean line calculation). Figure 4 shows the input mean swirl schedule, and the resulting impeller geometry is given in Table I. The radial velocity component W_r at midchord and midspan, plotted in Figure 5, shows that the mean and periodic parts of the velocity are of the same order. The relative Mach number on the blades varies between 0·76 on the suction side and 0·04 on the pressure side, as shown in Figure 6.

The second example is that of a typical low-speed inflow radial turbine impeller having 17 blades stacked at midchord (the hub and shroud profiles are courtesy of Dr. J. E. Borges). The flow is assumed to be incompressible and the blades' thickness varies linearly with the radial co-

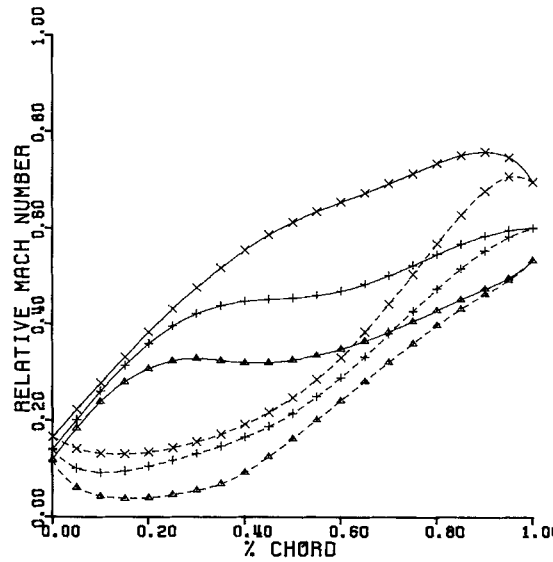

Figure 6. The relative Mach number on the blade suction (solid lines) and pressure (broken lines) surfaces, along the hub (Δ), midspan (+) and shroud (×) (every other node shown)

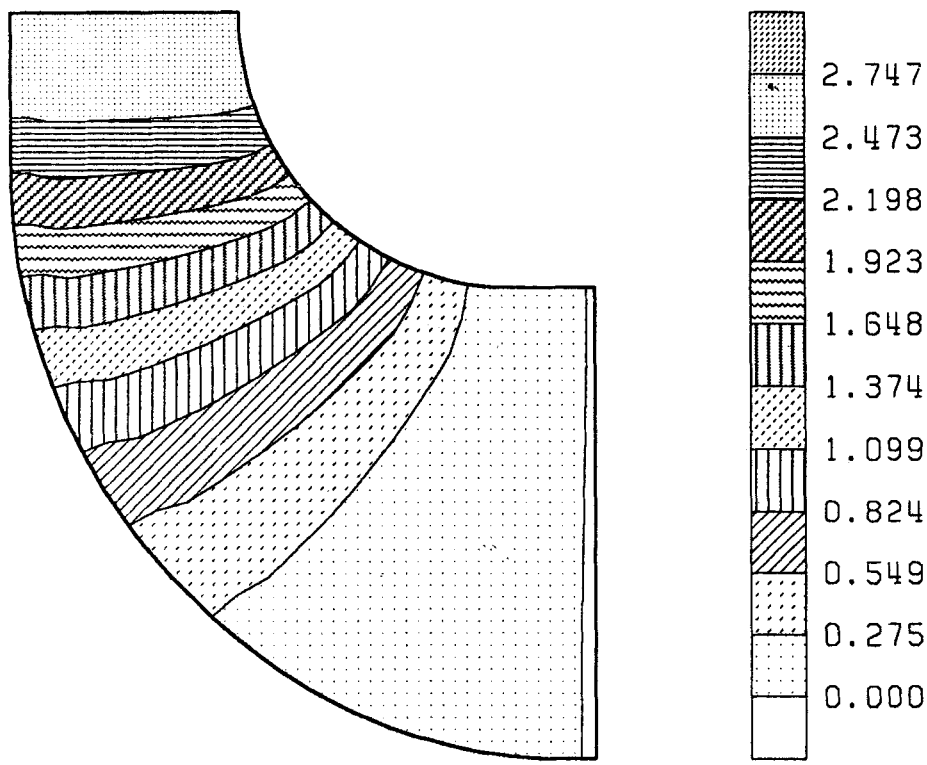

Figure 7. The mean swirl distribution $r\bar{V}_\theta$ for an RIT impeller

Table II. The impeller geometry (r, f, z) corresponding to the second design

r	f	z	r	f	z	r	f	z
1·0000	−0·1269	0·6129	0·8863	−0·0720	0·6129	0·7617	0·0013	0·6083
1·0000	−0·1258	0·5930	0·8863	−0·0732	0·5922	0·7645	−0·0052	0·5851
1·0000	−0·1226	0·5731	0·8863	−0·0768	0·5716	0·7673	−0·0246	0·5619
1·0000	−0·1220	0·5532	0·8904	−0·0777	0·5509	0·7765	−0·0209	0·5395
1·0000	−0·1158	0·5333	0·8945	−0·0710	0·5303	0·7858	−0·0152	0·5171
1·0000	−0·1100	0·5134	0·8986	−0·0667	0·5096	0·7951	−0·0094	0·4947
1·0000	−0·1047	0·4935	0·9027	−0·0629	0·4889	0·8043	−0·0074	0·4724
1·0000	−0·1006	0·4737	0·9069	−0·0607	0·4683	0.8136	−0·0064	0·4500
1·0000	−0·0982	0·4538	0·9110	−0·0604	0·4476	0·8229	−0·0087	0·4276
1·0000	−0·0965	0·4339	0·9151	−0·0616	0·4270	0·8321	−0·0140	0·4053
1·0000	−0·0965	0·4140	0·9192	−0·0637	0·4063	0·8414	−0·0200	0·3829
1·0000	−0·0930	0·3941	0·9243	−0·0624	0·3859	0·8527	−0·0210	0·3616
1·0000	−0·0918	0·3742	0·9294	−0·0620	0·3655	0·8640	−0·0213	0·3404
0·6303	0·0345	0·5783	0·5022	0·0000	0·5182	0·3858	−0·1294	0·4272
0·6390	0·0288	0·5528	0·5182	0·0000	0·4920	0·4100	−0·1253	0·4026
0·6477	0·0116	0·5273	0·5342	0·0000	0·4658	0·4343	−0·1132	0·3780
0·6631	0·0140	0·5042	0·5565	0·0000	0·4435	0·4636	−0·1103	0·3584
0·6785	0·0248	0·4811	0·5788	0·0000	0·4212	0·4928	−0·1104	0·3389
0·6940	0·0266	0·4580	0·6011	0·0000	0·3989	0·5221	−0·1074	0·3193
0·7094	0·0263	0·4349	0·6234	0·0000	0·3766	0·5514	−0·1022	0·2998
0·7249	0·0261	0·4118	0·6457	0·0000	0·3543	0·5806	−0·0947	0·2802
0·7403	0·0233	0·3887	0·6680	0·0000	0·3320	0·6099	−0·0869	0·2607
0·7557	0·0163	0·3656	0·6902	0·0000	0·3098	0·6391	−0·0745	0·2411
0·7712	0·0091	0·3425	0·7125	0·0000	0·2875	0·6684	−0·0625	0·2216
0·7894	0·0062	0·3219	0·7378	0·0000	0·2696	0·7001	−0·0521	0·2084
0·8076	0·0053	0·3013	0·7631	0·0000	0·2517	0·7319	−0·0486	0·1952
0·2900	−0·3644	0·3073	0·2279	−0·7205	0·1573	0·2129	−1·1123	0·0000
0·3241	−0·3581	0·2866	0·2694	−0·7066	0·1472	0·2543	−1·0871	0·0000
0·3582	−0·3390	0·2659	0·3109	−0·6648	0·1371	0·2957	−1·0116	0·0000
0·3935	−0·3230	0·2512	0·3508	−0·6231	0·1291	0·3371	−0·9415	0·0000
0·4289	−0·3060	0·2366	0·3907	−0·5776	0·1212	0·3785	−0·8712	0·0000
0·4643	−0·2860	0·2219	0·4306	−0·5297	0·1133	0·4199	−0·8018	0·0000
0·4996	−0·2669	0·2073	0·4704	−0·4858	0·1053	0·4613	−0·7370	0·0000
0·5350	−0·2428	0·1926	0·5103	−0·4386	0·0974	0·5027	−0·6707	0·0000
0·5704	−0·2199	0·1780	0·5502	−0·3942	0·0895	0·5441	−0·6086	0·0000
0·6057	−0·1932	0·1633	0·5901	−0·3492	0·0815	0·5855	−0·5470	0·0000
0·6411	−0·1697	0·1487	0·6299	−0·3101	0·0736	0·6269	−0·4816	0·0000
0·6777	−0·1477	0·1420	0·6698	−0·2755	0·0736	0·6683	−0·4348	0·0000
0·7143	−0·1403	0·1354	0·7097	−0·2640	0·0736	0·7097	−0·4192	0·0000

ordinate r in the form $t = 0{\cdot}01 + 0{\cdot}03(1-r)$ and vanishes along the blades' LE and TE; consequently the mean stream surface thickness parameter b $(= 1 - Bt/2\pi r)$ varies between 0·5725 and 1. The exponent $a(R)$ in equation (35) varies linearly between 2 along the hub and 0 along the shroud. The input mean swirl schedule and the resulting blade shape are given in Figure 7 and Table II respectively.

It is worth noting that the velocity at the blade suction or pressure surface may be calculated as follows:

$$\mathbf{W}^{+} = \mathbf{W}_{\mathrm{bl}} \pm \tfrac{1}{2}\Delta\mathbf{W},$$

where $\Delta\mathbf{W}$ is the velocity jump across the blade and may be calculated from the bound vorticity.[2]

These examples show that this technique can handle situations where the maximum Mach number is close to the transonic regime and where the periodic part of the velocity (which is a good measure of the discrete blade effect) is as large as the mean part.

5. CONCLUDING REMARKS

An analytical method to design turbomachinery blading in three-dimensional flow is presented. The numerical technique used to implement the design of turbomachinery blading in the subsonic regime has been described. A mixed spectral finite element scheme is used to solve the resulting governing equations, which are three-dimensional and of the elliptic type for subsonic flow. Since the problem is non-linear, the final blade shape corresponding to a prescribed mean swirl distribution is determined iteratively.

In the course of this work it was found that, for a given hub and shroud geometry, number of blades and their stacking position, and a mean swirl schedule that satisfies the zero incidence angle at the leading edge and the Kutta condition at the trailing edge, a converged solution for the blade shape is obtained when the mean meridional velocity does not vanish and the Mach number is not close to unity.

To demonstrate the application of the method, it is used to design two radial inflow turbine impellers. Some sample results for the blade shape, velocity and Mach number fields that would yield a prescribed mean swirl schedule are presented.

ACKNOWLEDGEMENTS

The author is grateful to Professor Sir W. R. Hawthorne and Dr. C. S. Tan of MIT for their valuable suggestions during the course of this work, and to Dr. C. S. Tan for revising and commenting on this paper. This work has been supported by Cummins Engine Company, Inc., when the author was working on his Ph.D. program at MIT. The cases presented in this paper were run on the mainframe of the Ecole Polytechnique de Montreal.

APPENDIX: NOMENCLATURE

b	mean stream surface thickness parameter, equation (17)
B	number of blades
$\mathbf{e}$	unit vector
f	blade shape
H	enthalpy
l	element characteristics dimension, e.g. its diagonal
m	distance along streamlines of the mean flow
P	pressure
(r, θ, z)	cylindrical co-ordinates
Se	entropy
t	blade thickness in the θ-direction
T	temperature
$\mathbf{V}$, $\mathbf{W}$	absolute, relative velocity vectors
$\tilde{\mathbf{v}}$	absolute periodic velocity vector
$S(\alpha)$	sawtooth function, equation (14)

Greek letters

α	blade surface, equation (8)
γ	specific heats ratio
$\delta_p(\alpha)$	periodic delta function, equation (9)
ρ	density
ρ_{av}	average density, equation (17)
Ψ	Stokes streamfunction, equation (19)
$\tilde{\Phi}$	periodic scalar potential function harmonics, equation (23)
ϕ	scalar potential function, equation (11)
$\mathbf{\Omega}$	vorticity vector
ω	impeller rotational speed
λ	pseudo-time step, equation (34)

Subscripts

bl	'at' the blade
LE	leading edge
m	meridional plane, r–z plane in Figure 1(a)
r, θ, z	r-, θ-, z-components
st	stacking position
TE	trailing edge
t	total, stagnation

Superscripts

$+/-$	blade pressure/suction surface, Figure 1(b)
*	rotary

Other

$\bar{(\ )}$	tangential average, equation (10)
$\tilde{(\ )}$	periodic part
RIT	radial inflow turbine
FEM	finite element method

REFERENCES

1. W. R. Hawthorne, C. Wang, C. S. Tan and J. E. McCune, 'Theory of blade design for large deflections: Part I—Two-dimensional cascade', *J. Eng. Gas Turbines and Power*, **106**, 346–353 (1983).
2. C. S. Tan, W. R. Hawthorne, J. E. McCune and C. Wang, 'Theory of blade design for large deflections: Part II—Annular cascades', *J. Eng. Gas Turbines and Power*, **106**, 354–365 (1983).
3. C. S. Tan, C. Wang, J. E. McCune and W. R. Hawthorne, 'Three dimensional blade design for large deflections using an analytic theory', *GT&PDL Report No. 168*, MIT, 1982; also *CUED/A—Turbo/TR 115*, Cambridge University, 1982.
4. W. R. Hawthorne, 'The actuator duct representation of turbomachinery blade rows', *CUED/A—Turbo/TR 119*, Cambridge University, 1983.
5. T. Q. Dang and J. E. McCune, 'Design methods for highly-loaded blades with blockage in cascade', in P. M. Sockol and K. N. Ghia (eds), *Symp. on Computation of Internal Flows: Methods and Applications*, 1984, pp. 129–136.
6. T. Q. Dang, A three-dimensional blade design method to control secondary flow', *Ph.D. Thesis*, MIT, 1985.
7. J. E. Borges, 'Three-dimensional design in turbomachinery', *Ph.D. Thesis*, Cambridge University, 1986.

8. H. Lamb, *Hydrodynamics*, 6th Edn. Dover, New York, 1945.
9. W. S. Ghaly, 'A study and design of radial turbomachinery blading in three-dimensional flow', *Ph.D. Thesis*, MIT, 1986.
10. M. J. Lighthill, *An Introduction to Fourier Analysis and Generalized Functions*, Cambridge University Press, Cambridge, 1966.
11. G. Strang and G. J. Fix, *An Analysis of the Finite Element Method*, Prentice-Hall, Englewood Cliffs, NJ, 1973.
12. G. F. Carey and J. T. Oden, *Finite Elements: A Second Course*, Prentice-Hall, Englewood Cliffs, NJ, 1983.
13. O. C. Zienkewicz, *The Finite Element Method*, McGraw-Hill, New York, 1977.
14. G. F. Carey and J. T. Oden, *Finite Elements: Computational Aspects*, Prentice-Hall, Englewood Cliffs, NJ, 1983.
15. G. Dahlquist and A. Bjorck, *Numerical Methods*, Prentice-Hall, Englewood Cliffs, NJ, 1974.
16. J. W. Cooley and J. W. Tukey, 'An algorithm for the machine calculation of complex Fourier series', *Math. Comput.*, **19,** 297 (1965).
17. C. Lanczos, *Discourse on Fourier Series*, Oliver & Boyd, London, 1966.
18. D. Potter, *Computational Physics*, Wiley, New York, 1972.